Catalysis Science & Technology

Accepted Manuscript

ROYAL SOCIETY OF CHEMISTRY

www.rsc.org/catalysis

High Efficiency new Visible Light Driven Ag_2MoO_4-Ag_3PO_4 Composite Photocatalyst towards Degradation of Industrial Dyes

Rengasamy Dhanabal (*), Sivan Velmathi (†) and Arumugam Chandra Bose (*)

(*) Nanomaterials Laboratory, Department of Physics, National Institute of Technology, Tiruchirappalli - 620 015 India

(†) Organic and Polymer Synthesis Laboratory, Department of Chemistry, National Institute of Technology, Tiruchirappalli - 620 015 India

ABSTRACT:

High efficiency new visible light driven Ag_2MoO_4-Ag_3PO_4 composite photocatalysts with different weight ratios were successfully synthesized by a facile solution based in-situ preparation method and characterized using X-ray diffraction (XRD), X-ray photoelectron spectroscopy (XPS), scanning electron microscopy (SEM), Fourier transform infrared spectroscopy (FTIR), UV-visible diffuse reflectance spectroscopy (UV-vis DRS), photoluminescence spectroscopy (PL), and zeta potential measurement. Under visible light irradiation, the 10 wt% of Ag_2MoO_4-Ag_3PO_4 composite photocatalyst exhibits enhanced photocatalytic degradation efficiency compared to other composites of Ag_2MoO_4-Ag_3PO_4, pure Ag_3PO_4 and pure Ag_2MoO_4 for degradation of methylene blue (cationic dye). The 10 wt% of Ag_2MoO_4-Ag_3PO_4 composite photocatalyst is further used to investigate the photocatalytic degradation of rhodamine B (cationic dye) and methyl orange (anionic dye). The higher photocatalytic degradation efficiency of 10 wt% Ag_2MoO_4-Ag_3PO_4 towards cationic dye is closely related to its surface potential and the observed degradation efficiency of MB is 2.7 and 16.87 times higher than RhB and MO respectively. Based on the bandgap alignment, the photocatalytic degradation mechanism of Ag_2MoO_4-Ag_3PO_4 composite photocatalysts was examined. In addition, the quenching effect of different scavenger test

displays, holes and $O_2^{-\bullet}$ are the most reactive species which plays major role on photocatalytic degradation of MB. The UV-vis DRS and photoluminescence study are also supported the higher photocatalytic degradation. TOC analysis was done to confirm the mineralization of dyes. The Ag_2MoO_4-Ag_3PO_4 composite photocatalyst is highly stable and 89% of MB photocatalytic degradation was achieved after 4 recycle measurements under visible light irradiation. In addition, no phase changes of Ag_2MoO_4-Ag_3PO_4 composite photocatalyst and degraded product was confirmed.

Keywords:

Ag_2MoO_4, Ag_3PO_4, Electrostatic force, Mulliken electronegativity, Industrial dyes.

1. INTRODUCTION

The disposal of industrial garbage especially dyes from the textile industry has been a problem in the past few decades. The semiconductor photocatalysis has gained attention as a significant solution to many potential applications such as hydrogen production from the water splitting, degradation of organic toxic pollutants and water purification and disinfection [1-3]. Among them, the degradation of organic pollutants using semiconductors have played a crucial role because of its promising, environmental, and cost effective technology for treatment of contaminated groundwater and wastewater [2,4]. Since, the discovery of the Honda-Fujishima effect in the early 1990s, the TiO_2 has been used to study the photocatalytic degradation of dyes under ultraviolet light irradiation (UV light) [5-7]. However, TiO_2 (3.2 eV) can only absorb UV light which accounts for only 4 % of solar radiation reaching the earth thereby greatly restricting its practical applications under solar light [8]. So, in the technological perspective it is important to develop visible light active material to investigate the photocatalytic degradation of organic pollutants. Many researchers have focused on the development of single phase semiconductor materials [Ag_2WO_4, $Ag_6Si_2O_7$, TiO_2 and WO_3]

and its photocatalytic degradation under visible light [9-11]. In addition, the coupling of semiconductor with another semiconductor in the form of composite materials with matched band edge potential (SnO_2-Fe_2O_3, Bi_2O_3-Bi_2WO_6, WO_3-$Ca_2Fe_3O_4$, Cu_2O-ZnO, RGO-TiO_2, CuO-$BiVO_4$, $BiVO_4$-Bi_2O_3, $LaVO_4$-TiO_2,Bi_2O_3-ZnO, BiOI-BiOCOOH and $Fe_2(MoO_4)_3$-MoO_3) is another way to promote photogenerated electron-hole pair and thus increasing separation of electron-hole pair efficiency as well as inhibiting their rate of electrons-holes recombination [12-22].

Recently, Yi et al., reported the use of Ag_3PO_4 as an excellent photocatalyst material to oxidize water and decompose the organic contaminants in aqueous solutions under visible light irradiation (λ= 420 nm) [23]. The strong valence band potential of Ag_3PO_4 was reasoned for excellent water oxidization and degradation of organic dyes [24]. The further investigation on preparation of shape, morphology and crystal face of Ag_3PO_4 greatly enhance the photocatalytic activity. However, the conduction band potential of Ag_3PO_4 (0.45 eV vs NHE) is more positive than that of H_2-H^+, which limits its application in hydrogen production from water splitting. Moreover, Ag_3PO_4 composites have been developed by coupling with wide bandgap semiconductors ($In(OH)_3$, SnO_2, CeO_2, and TiO_2, etc.) [25-28], narrow bandgap semiconductors (Bi_2WO_6, CdS and BiOI etc.) [29-31] and carbon materials (RGO, multiwall nanotube and quantum dots) [32-34]. Lei Liu et al., [35] have reported the photocatalytic activity of GO-Ag_3PO_4 system, the GO sheets could facilitate charge transfer and suppress the recombination of electron-hole pair thus enhance the efficiency and stability of Ag_3PO_4. Yuyu Bu et al., [36] prepared Ag_3PO_4 nanoparticles on the surface of PANI by in situ deposition method and they found that the existence of interfacial electric field formed at interface of Ag_3PO_4 and PANI can dramatically enhance the separation efficiency of the photogenerated electron-hole pairs which improves the photocatalytic degradation performance and stability of the system. The g-C_3N_4/Ag_3PO_4 composite photocatalyst is

developed and the improved photocatalytic performance and stability is due to synergistic effects such as structural stability, charge transfer process, high surface area and adsorption ability between g-C_3N_4 and Ag_3PO_4 composites system [37].The high electrical conductivity of carbon materials ultimately inhibits the electron-hole recombination which enhances the photocatalytic activity of Ag_3PO_4 composites. The use of wide bandgap semiconductors such as AgBr [38] and AgI [39] with Ag_3PO_4 are potential candidate to improve the optical absorption property of Ag_3PO_4 which leads to superior photocatalytic degradation.

In this paper, the Ag_2MoO_4 (low absorbance in visible light) [40] with strong oxidation potential than AgI and AgBr was chosen to develop highly stable and novel Ag_2MoO_4/Ag_3PO_4 composite photocatalyst. The pure phase of Ag_2MoO_4 was introduced to Ag_3PO_4, in order to further enhance the photo-oxidation property of Ag_3PO_4 towards photocatalytic degradation of dyes. The Ag_2MoO_4 with wide bandgap was considered for the efficient charge separation due to their matched band edge potentials of Ag_2MoO_4-Ag_3PO_4 composite photocatalyst. Initially, the Ag_2MoO_4-Ag_3PO_4 with different weight ratios of Ag_2MoO_4 was prepared from MoO_3. Then, all samples were characterized by various analysing techniques such as XRD, XPS, SEM, FTIR, UV-vis DRS, PL, and zeta potential measurement. Second, the photocatalytic activity of as-prepared pure Ag_3PO_4, Ag_2MoO_4-Ag_3PO_4 composites and pure Ag_2MoO_4 were evaluated through photocatalytic degradation of cationic dyes (MB, RhB) and anionic dye (MO). In addition, photogenerated electron-hole transfer process was illustrated based on the bandgap alignment of Ag_2MoO_4-Ag_3PO_4 composite and its catalytic activity. Also, the trapping of reactive species measurement, PL and UV-vis DRS studies were correlated to photocatalytic activity of composites. TOC analysis was done to confirm the mineralization of the dyes. Finally, the systematic investigation on recyclability, stability and identification of degraded final product of Ag_2MoO_4-Ag_3PO_4 composite was examined after photocatalytic measurement.

2. EXPERIMENTAL SECTION

2.1 Chemicals.

The ammonium heptamolybdate tetrahydrate ($(NH_4)_6Mo_7O_{24}\cdot 4H_2O$)), nitric acid - HNO_3 (69 %), ammonia solution (25 %), methylene blue (MB), rhodamine B (RhB) and methyl orange (MO) were purchased from Merck, India. Silver nitrate ($AgNO_3$) and Di sodium phosphate (Na_2HPO_4) were purchased from Alfa Aesar, United Kingdom. All the chemicals were of analytical grade and used without any further purification. The double distilled water was used in all experiments.

2.2 Preparation of MoO_3.

The MoO_3 crystal was synthesized using precipitation method [41]. In typical procedure, 0.2 M of ammonium heptamolybdate tetrahydrate (AHM) was dissolved in 10 mL of double distilled water. A homogeneous solution was obtained after stirring for 10 min and 5 mL of HNO_3 was added dropwise into the solution. Then the mixture was heated to 120 °C for 3 h in oil bath and resulting precipitate was subsequently centrifuged and washed with several times by double distilled water. The obtained MoO_3 powder was dried at 80 °C for 6 h in hot air oven.

2.3 Preparation of Ag_2MoO_4-Ag_3PO_4 composite photocatalyst.

The Ag_2MoO_4-Ag_3PO_4 composites photocatalysts were prepared as follows: The solution A and solution B were prepared separately. An appropriate amount of as-prepared MoO_3 was added to 50 mL of double distilled water with sonication for 30 min to form uniform MoO_3 dispersion. Then, the 5 mL of $NH_3.H_2O$ was added into MoO_3 dispersion to form $(NH_4)_2MoO_4$. In addition, 0.3 M of $AgNO_3$ also was dissolved into above mixture (solution A) and stirred for 30 min. On the other hand, 0.1 M of Na_2HPO_4 was dissolved in 50 mL of water (solution B). Then, the solution B was added dropwise into former solution of A. The solution pH was adjusted to 7.5 by simultaneous addition of 1 mL HNO_3 indicated the

formation of yellow colored Ag_2MoO_4-Ag_3PO_4 composite photocatalyst and solution was further stirred for 4 h under dark condition. Finally, the precipitates were centrifuged and washed several times with double distilled water. The obtained solid product of Ag_2MoO_4-Ag_3PO_4 was dried at 100 °C for 6 h in hot air oven. The amount of MoO_3 was changed as 5 wt%, 10 wt% and 15 wt% to synthesize different weight ratio of Ag_2MoO_4-Ag_3PO_4 composites. For comparison, the pure Ag_3PO_4 and Ag_2MoO_4 were also prepared without addition of MoO_3 and Na_2HPO_4, respectively by following the same experimental procedure.

2.4 Characterizations

The phase identification of as-prepared Ag_2MoO_4-Ag_3PO_4 composite photocatalysts was performed using Ultima III Rigaku X-ray diffractometer (XRD) with scanning rate 4°/min, step size 0.02°/min, Cu $K\alpha_1$ radiation, λ =1.5406 Å in a 2θ range from 10 to 80º at room temperature. The X-ray photoelectron spectroscopy was used to investigate the binding energies of the Ag_2MoO_4-Ag_3PO_4 composite photocatalysts. The morphologies of Ag_2MoO_4/Ag_3PO_4 composite photocatalysts were characterized by VEGA3 TESCAN scanning electron microscope (SEM). The Ag_2MoO_4-Ag_3PO_4 composite photocatalysts were mixed with KBr (Loba chemicals, India) to prepare the pellets for the FTIR measurements using Thermo-Scientific NICOLET iS5 Fourier transform infrared spectrometer (USA). UV-Visible diffuse reflectance spectrum was recorded using JASCO UV-Vis NIR spectrophotometer (Model-V-670, USA) in the range of 300 nm - 800 nm. Room temperature photoluminescence spectra of composites were obtained using JASCO spectroflurometer (Model – 8500, USA) with excitation wavelength of 325 nm. The zeta potential measurement was carried out using Zetasizer (Model- MAL1052893, United Kingdom). Finally, to determine the mineralization of dyes, the changes in total organic carbon was carried using total organic carbon analyser (TOC-L, Shimadzu, Japan).

2.5 Photocatalytic experiment and detection of reactive oxygen species.

The photocatalytic dye degradation of Ag_2MoO_4/Ag_3PO_4 composite photocatalyst was investigated using various organic dyes namely MB, RhB and MO under visible light irradiation. 0.1 g of each photocatalyst was added into 1 L of double distilled water containing 10 mg of MB, RhB, and MO dye powder, separately. The photocatalytic chamber consists of tungsten halogen lamp and reactions are carried out under visible light irradiation with an E = 350 W and $\lambda \geq 420$ nm at ambient temperature. Prior to irradiation, the suspension was magnetically stirred for 30 min in the dark condition to establish the adsorption-desorption equilibrium on the surface of catalysts. Finally, at the given time interval the 4 mL of catalyst containing suspension was centrifuged and used to measure the change in concentration using UV-Vis spectrophotometer (UV-2600, Shimadzu, Japan) ranging from 250 nm to 800 nm.

3. RESULTS AND DISCUSSION

3.1 Characteristics of Ag_2MoO_4-Ag_3PO_4 composites.

Figure 1 shows the XRD pattern of as-synthesized Ag_3PO_4 and Ag_2MoO_4/Ag_3PO_4 composite photocatalysts, in which five sets of XRD patterns are obtained: those unmarked were indexed to the body centered cubic Ag_3PO_4 structure corresponding to the JCPDS NO: 06-0505, whereas other peaks marked with ♦ were assigned to the face centred cubic Ag_2MoO_4 structure corresponding to the JCPDS NO: 75-0250. The intensity of diffraction peaks of Ag_2MoO_4 composites increases gradually with MoO_3 content supported the strong coexistence of Ag_2MoO_4 along with Ag_3PO_4. This XRD pattern suggests that both Ag_2MoO_4 and Ag_3PO_4 were formed and these results ruled out the possibility of any third phase formation, indicating Ag_3PO_4, Ag_2MoO_4 and Ag_2MoO_4-Ag_3PO_4 composites have been successfully prepared.

The surface composition and chemical state of as-prepared 10wt% Ag_2MoO_4/Ag_3PO_4 composite was investigated by X-ray photoelectron spectroscopy (XPS) and the results are depicted in Figure 2. Figure 2 (a) shows the XPS survey spectrum of as-prepared 10wt% Ag_2MoO_4-Ag_3PO_4 confirming the presence of Ag, Mo, P and O. In addition, the carbon peak C (1s) at binding energy 284.6 eV was assigned to hydrocarbon from the instrument [42]. Figure 2 (b) comprises two individual peaks at binding energy 374.5 eV and 368.4 eV, which could be ascribed to spectra of Ag ($3d_{3/2}$) and Ag ($5d_{5/2}$) [43]. Also, the two distinct peaks were observed at binding energies 235.4 eV and 232.29 eV corresponding to Mo ($3d_{3/2}$) and Mo ($3d_{5/2}$) as shown in Figure 2 (c) [40]. The P (2p) peak located at binding energy ~ 133 eV is due to P^{5+} in PO_4^{3-} [40] as shown in Figure 2 (d). The deconvolution spectra for O (1s) is shown in Figure 2 (e).The two peaks at binding energies 532.1 eV and 530.4 corresponds to oxygen, hydroxyl groups in the sample and are in good agreement with already reported results [44]. No other peak was observed suggesting that successful formation of Ag_2MoO_4-Ag_3PO_4 composite photocatalysts.

The morphology and elemental analysis were investigated by SEM with EDS technique. The SEM images of as-prepared pure Ag_3PO_4, pure Ag_2MoO_4 and Ag_2MoO_4-Ag_3PO_4 composite are shown in Figure 3 (a-c). The morphology of pure Ag_3PO_4 was ascertained to be an irregular sphere shaped particles (Figure 3a) with size ranging from 294 nm to 1.5 μm (calculated from inset Figure 3(a)). The as-prepared pure Ag_2MoO_4 shows agglomerated cubic and irregular morphology with 1.9 μm - 5.5 μm in size (Figure 3(b)). Inset of Figure 3b exhibits magnified cubic shaped morphology of Ag_2MoO_4. Figure 3c clearly explains presence of both cubic shaped Ag_2MoO_4 and sphere shaped Ag_3PO_4 particles and are well connected. The EDS spectra of pure Ag_3PO_4 and 10 wt % Ag_2MoO_4-Ag_3PO_4 composite are shown in Figure 3(d-e). The presence of Ag, P and O for pure Ag_3PO_4 and Ag, P, O and Mo were identified for Ag_2MoO_4 which further confirming the presence of Mo in

Ag_2MoO_4. Table 1 and Table 2 show the elemental composition of Ag, P, O and Mo in pure Ag_3PO_4 and 10 wt % Ag_2MoO_4-Ag_3PO_4 composite.

The FTIR spectra of as-prepared Ag_3PO_4 and Ag_3PO_4-Ag_2MoO_4 composites are represented in Figure 4 (a). In the FTIR spectrum of pure Ag_3PO_4, the bands at 3424 cm^{-1} and 1651 cm^{-1} indicates stretching and bending vibration of OH^- ions adsorbed on the surface. Two strong bands are observed at 1013 cm^{-1} and 551 cm^{-1} corresponding to P-O stretching vibrations of PO_4^{3-} [37]. In the case of 5, 10, and 15 wt % of Ag_2MoO_4-Ag_3PO_4 composites, new peak observed at 828 cm^{-1} is assigned to stretching vibration of O-Mo-O [40]. Thus, FTIR spectra reveal the formation of Ag_2MoO_4 on the Ag_3PO_4 composites.

The UV-Visible diffuse reflectance spectra of as-prepared pure Ag_3PO_4, pure Ag_2MoO_4 and Ag_2MoO_4/Ag_3PO_4 composites are shown in Figure 4 (b). The Ag_3PO_4 exhibits optical absorption in the range 450-530 nm while Ag_2MoO_4 shows broad absorption from 335 nm to 430 nm in which a broad peak appears from 335-398 nm at UV region, and another peak shows at 400 nm- 430 nm at visible region. This result explains the major light absorption is from UV region and also exhibits low absorbance in the visible region. Similar kind of observation was proposed by Hao Jiang et al [40]. For Ag_2MoO_4/Ag_3PO_4 composites, the strong visible light absorption is observed for all samples. The bandgap (E_g) of all samples can be calculated using Kubleka-Munk function is shown in equation (1).

$$F(R_\infty) = \frac{(1-R_\infty)^2}{2R_\infty} = \frac{K(\lambda)}{s(\lambda)} \propto \alpha = \frac{(h\upsilon - E_g)^2}{h\upsilon} \quad (1)$$

Where $F(R_\infty)$ is the K-M function, R_∞ is the diffuse reflectance of an infinitely thick sample, $K(\lambda)$ is the absorption coefficient, $s(\lambda)$ is the scattering coefficient, $h\upsilon$ is the photon energy and E_g is the bandgap energy of direct transition, respectively. The bandgap was derived from the plot between the square of the K-M function $F(R)^2$ and energy. To obtain the optical bandgap, the linear part of $F(R)^2$ curve was extrapolated and intersected to the

energy axis. The calculated bandgap is 2.35 eV, 3.05 eV (inset Figure 4 (c)), 2.41 eV, 2.42 eV and 2.38 eV corresponding to as-prepared pure Ag_3PO_4, pure Ag_2MoO_4, 5 wt% Ag_2MoO_4-Ag_3PO_4, 10 wt % Ag_2MoO_4-Ag_3PO_4 and 15 wt % Ag_2MoO_4-Ag_3PO_4 respectively as shown in Figure 4 (c). In addition, it is noted, the bandgap of 15wt% Ag_2MoO_4/Ag_3PO_4 is slightly increased to the pure Ag_3PO_4 but decreased when compared with 5wt% and 10 wt% Ag_2MoO_4/Ag_3PO_4 composite. This might have caused by the poor interfacial interaction of Ag_2MoO_4 with Ag_3PO_4 may due to aggregation of Ag_2MoO_4 at higher amount loading [45].

The photoluminescence (PL) emission spectra is used to investigate the migration and separation efficiency of photogenerated electrons and holes. In general, the strong intensity of the fluorescence means that the photogenerated electrons and holes are prone to recombination and the lifetime of the photogenerated electrons are short. However, the weak intensity of the generated fluorescence means that the separation of electrons and holes are high resulting in a longer lifetime of the photogenerated electrons and holes [46-47]. Figure 4 (d) shows the PL spectra of as-prepared pure Ag_3PO_4 and Ag_2MoO_4-Ag_3PO_4 composites measured at an excitation wavelength of 325 nm. For pure Ag_3PO_4, a broad emission peak was observed at 390 to 510 nm corresponds to photoexcited electrons on the conduction band recombining with valence band holes which is approximately equal to the bandgap of material. For the case of Ag_2MoO_4-Ag_3PO_4 composites, the fluorescence intensity was weakened from 5 wt% to 10 wt% Ag_2MoO_4-Ag_3PO_4 and start rising back to 15 wt% of Ag_2MoO_4-Ag_3PO_4 as shown in Figure 4 (d). This indicates that presence of 10 wt% Ag_2MoO_4 can effectively prevent the annihilation of photogenerated electron - hole pairs and improves separation efficiency and life time of photogenerated electrons and holes [48-50].

The surface energy of composite materials was analyzed using zeta potential measurement as shown in Figure 5 (a-c). The negative surface potential of -44.4 mV, - 50.2

mV, – 50.5 mV were observed for 5 wt% Ag_2MoO_4-Ag_3PO_4, 10 wt% Ag_2MoO_4-Ag_3PO_4 and 15 wt% Ag_2MoO_4-Ag_3PO_4 composites, respectively.

3.2 Photocatalytic degradation of pure Ag_3PO_4, Ag_2MoO_4 and Ag_2MoO_4-Ag_3PO_4 composites

The photocatalytic activity of pure Ag_3PO_4, pure Ag_2MoO_4 and Ag_2MoO_4-Ag_3PO_4 composite photocatalyst was evaluated through the photocatalytic degradation of cationic dye (MB, RhB) and anionic dye (MO) under visible light irradiation. All these dyes are well known water pollutants and are discharged from textile industries. Initially, two set of experiments were carried out to investigate the nature of dyes and catalyst. The first experiment was carried out to confirm the self photolysis of dye where the aqueous medium of dyes (separate reaction was done to each dye) was exposed under visible light irradiation. It is observed that there is no colour change in MB, RhB and MO up to 35 min of visible light irradiation as shown in Figure 6. This result confirms the self photolysis of dyes in the presence of visible light irradiation is ignored. The second experiment was performed where appropriate amount of catalyst was mixed with aqueous solution of dyes to study the influence of catalyst under dark condition. It could be observed that very minimum percentage (4 %) of degradation was observed for all dyes under dark condition up to 30 min. The observed minimum percentage is due to chemi-adsorption of dyes on the surface of material which is negligible. So the visible light irradiation was used for photocatalytic degradation of dyes. The as-prepared samples of pure Ag_3PO_4, pure Ag_2MoO_4 and Ag_2MoO_4-Ag_3PO_4 (from 5 wt% to 15 wt %) composite photocatalysts have been used to degrade MB. Using, pure Ag_3PO_4, Ag_2MoO_4-Ag_3PO_4 and pure Ag_2MoO_4 the aqueous solution of MB was degraded after visible light irradiation which is confirmed from gradual decrement in characteristic absorption peak intensity (λ_{max}) at 665 nm, 605 nm and 250 nm

and ultimately the peaks disappeared (see Figure 7). The percentage of photocatalytic degradation was calculated using equation (2)

$$\frac{C_o - C_t}{C_o} \times 100 \qquad \text{---------- (2)}$$

Where, C_o, C_t are the initial and residual concentrations of MB, RhB and MO at different interval times, respectively.

From the Figure 8 (a), as-prepared Ag_3PO_4 and Ag_2MoO_4-Ag_3PO_4 composite photocatalyst exhibited almost complete degradation under visible light irradiation. In comparison between Ag_2MoO_4-Ag_3PO_4 composite photocatalyst, pure Ag_3PO_4 and pure Ag_2MoO_4, the 5 wt% Ag_2MoO_4-Ag_3PO_4 takes 11 min to degrade 98.3 % of MB whereas 10 wt% Ag_2MoO_4-Ag_3PO_4 takes 8 min to degrade 98 % MB. However, the 15 wt% Ag_2MoO_4-Ag_3PO_4 takes 35 min to achieve 97.4 % of MB degradation. Among the photocatalyst used, 10 wt% Ag_2MoO_4-Ag_3PO_4 showed almost a complete degradation within 8 min whereas pure Ag_3PO_4, 5 wt% Ag_2MoO_4-Ag_3PO_4, 15 wt% Ag_2MoO_4-Ag_3PO_4 exhibited complete degradation within 35, 11 and 35 min, respectively. The pure Ag_2MoO_4 takes 180 min to degrade the 72% of MB. As the weight percentage of MoO_3 increased from 10 wt% to 15 wt %, the MB degradation of 15 wt% Ag_2MoO_4-Ag_3PO_4 is prolonging the visible light irradiation time. The possible reason for increase in degradation time is that number of Ag_2MoO_4 formed on the surface of Ag_3PO_4 is more, which decreases light absorbance on the Ag_3PO_4, and is isolated from the contact between Ag_3PO_4 and MB molecules. Since, sample 10 wt% Ag_2MoO_4-Ag_3PO_4 is considered as good catalyst, it is used to investigate the degradation of RhB and MO dye. Figure 8 (b) shows the degradation of RhB and MO using 10 wt% Ag_2MoO_4-Ag_3PO_4. The 99 % of RhB degradation was achieved within 22 min whereas 98 % of MO degradation was achieved within 135 min. This result suggests that MB degradation is 2.75 times higher than RhB degradation and 16.87 times higher than MO

degradation. As discussed, a minimum visible light irradiation time is required to achieve the complete degradation of cationic dye molecules such as MB and RhB whereas longer visible light irradiation time is needed for degradation of anionic dye like MO. The reason is explained based on the interaction between dye molecules (cationic and anionic) and nature of Ag_2MoO_4-Ag_3PO_4 composite photocatalyst. Figure 9 illustrates the interaction between dye molecules and Ag_2MoO_4-Ag_3PO_4 composite photocatalyst under visible light irradiation. The surface charge of dye molecules and Ag_2MoO_4-Ag_3PO_4 plays the key role in photocatalytic degradation of dyes. In general, it is noticed that cationic dyes such as MB and RhB could be bounded with positive charge while negative charge is bounded on the surface of anionic MO dye. In addition to note, the surface energy of Ag_2MoO_4-Ag_3PO_4 composites show a negative potential is to be - 44.4 mV, - 50.2 mV and - 50.2 mV for 5 wt%, 10 wt% and 15 wt% Ag_2MoO_4-Ag_3PO_4 composite, respectively (see Figure 5). Moreover, it could be inferred from the FTIR spectra, the peak at 1651 cm^{-1} is attributed to stretching vibration of OH^- ions, which also reveals that the as-obtained Ag_2MoO_4-Ag_3PO_4 composite inherits negative charge on the surface [51]. As shown in Figure 9, when Ag_2MoO_4-Ag_3PO_4 is in contact with dye molecules in aqueous medium, it tends to stabilize electrostatically and further the negative surface potential on the Ag_2MoO_4-Ag_3PO_4 composite photocatalyst facilitates the strong interaction due to electrostatic attraction between cationic dye molecules and Ag_2MoO_4-Ag_3PO_4 composite photocatalyst. The electrostatic attraction induces the strong interaction between positively bounded dye molecules and negatively charged Ag_2MoO_4-Ag_3PO_4 which causes the faster degradation of cationic dyes. Also, it could be explained that the better degradation of MB than RhB probably comes from complicated structure of RhB [52]. Moreover, in the case of anionic dye, there is an electrostatic repulsion which is due to interaction between negatively charged Ag_2MoO_4-Ag_3PO_4 composite and negatively bounded dye molecules. Ultimately, the longer irradiation time in

MO leads to slower degradation. Thus the cationic dye (RhB or MB) could be easily adsorbed on the catalyst surface by the electrostatic field, and charge transfer is facilitated. However, for the anionic dye (MO) this effect is not operative as such. Hence, Ag_3PO_4 catalyst is good at removing the cationic dyes efficiently.

In addition, to understand the influence of reactive species, trapping experiments and recyclability measurements are carried out on the photocatalytic degradation of MB over 10 wt% Ag_2MoO_4-Ag_3PO_4. The disodium ethylenediaminetetraacetate (Na_2-EDTA), p-benzoquinone (BZQ) and tert-butanol (t-BuOH,) were used as scavengers for holes, $O_2^{-\bullet}$ radicals and $^{\bullet}OH$ radicals, respectively. The concentration of all scavengers are used to be 1 mmol/L in the reaction system. The addition of 1 mM of Na_2-EDTA greatly suppresses the percentage of photocatalytic degradation from 98 % to 18 % in 8 min (Figure 10 (a)), whereas introduction of 1 mM of BZQ exhibited 48.82 % of photocatalytic degradation of MB. However, 61.02 % of photocatalytic degradation of MB was observed in the presence of 1 mM of t-BuOH in the system. This decreasing photocatalytic degradation efficiency clearly indicates that the holes are main reactive species playing an important role in the photocatalytic degradation of MB than $O_2^{-\bullet}$ and $^{\bullet}OH$ radicals. In comparison to $^{\bullet}OH$ radicals, the $O_2^{-\bullet}$ radicals have little more influence in the photocatalytic degradation. In recyclability measurement, after every 8 min of photocatalytic degradation, the catalyst was recollected by slow evaporation process at 60 °C and is used for recyclability measurement. The 89 % of MB photocatalytic degradation was achieved after 4 recycle measurements suggest that slight decrease in the efficiency and catalyst has significant photostability as shown in Figure 10 (b).

In order to study the robustness of 10 wt% Ag_2MoO_4-Ag_3PO_4 composite photocatalyst, XRD and FTIR studies were carried out after photocatalytic degradation reaction. The XRD and FTIR studies also performed after four successive experimental runs

and the results are depicted in Figure 10. It is observed that from Figure 10 (c), there is no obvious change in peak location before and after photocatalytic reaction indicated good stability and a decrement in peak intensity was observed suggesting declined crystallinity after photocatalytic reaction. Figure 10 (d) shows the FTIR spectra of different functional groups associated with pure MB, RhB and MO before and after visible light irradiation of 10 Ag_2MoO_4-Ag_3PO_4. In case of pure MB, the observed peaks at 3428 cm^{-1} (stretching vibration of H-OH), 1600 cm^{-1} (CH=N), 1500-1400 cm^{-1} (C=C), 1400-1300 cm^{-1} (-CH_2 or -CH_3), 1254 cm^{-1} (-C-N), 1222 cm^{-1}(N-N), 1200-1000 cm^{-1}(C-O), and 947 cm^{-1} (-N-O) are disappeared in the degraded sample as shown in Figure 10 (d-ii). The pure RhB exhibit peaks at 1588 cm^{-1}, 1693 cm^{-1}, and 1645 cm^{-1} corresponding to the characteristic of C-C stretching vibration in aromatic ring, C=O bands and C=N band vibration, respectively. Figure 10 (d-iv) shows the disappearance of the functional groups in the degraded sample [53]. The FTIR of MO shows peaks corresponding to the asymmetric stretching CH_3 vibrations at 2924.06 cm^{-1}, ring vibrations at 1036.7 cm^{-1}, and the -C-N band finger prints of the azo nature of dye at 1119.1 cm^{-1} and there distinct bands are absent in degraded sample [54] as shown in Figure 10 (d-vi). Hence, this FTIR study gives evidence for degradation of MB, RhB and MO dyes. The total organic carbon analysis (TOC) was carried out to determine changes in the total organic carbon of the dyes. For TOC measurement, the 10 wt% Ag_2MoO_4-Ag_3PO_4 composite is taken into account which is used to degrade MB, RhB and MO dye within 8 min, 22 min and 135 min illumination of visible light irradiation, respectively. The 5.730 ppm of MB is decreased into 3.994 ppm denotes degradation of 30.29 % of MB dye. For RhB, the 6.905 ppm is decreased to 3.837 ppm showed 44.43 % and the 7.765 ppm of MO is decreased into 5.617 ppm confirmed 27.66 % of degraded dyes. This indicates the dyes removed over 10 wt% Ag_2MoO_4-Ag_3PO_4 composite was mainly by mineralization. Since the carbon concentration in the final solution is lower than the dyes concentration.

3.3 Possible photocatalytic mechanism of Ag_3PO_4 - Ag_2MoO_4 composites

The conduction band (E_{CB}) and valence band (E_{VB}) edge potentials of Ag_2MoO_4-Ag_3PO_4 can be estimated using Mulliken electronegativity theory which is given in equation (3) and (4).

$$E_{VB} = \chi - E_0 + 0.5E_g \quad \text{----------} \quad (3)$$

$$E_{CB} = E_{VB} - Eg \quad \text{----------} \quad (4)$$

Where E_{VB} and E_{CB} are the valence and conduction band edge potentials, respectively; χ is electronegativity of the semiconductor, determined by the geometric mean of the absolute electronegativity of constituent atoms; E_o is the energy of free electrons on the hydrogen scale (about 4.5 eV); E_g is the bandgap of semiconductor material. The absolute electronegativity of both Ag_2MoO_4 and Ag_3PO_4 to be 5.90 and 5.96 eV, respectively [55, 39]. The E_{VB} values of Ag_3PO_4 and Ag_2MoO_4 were determined to be 2.635 and 2.925 eV, respectively and E_{CB} values of Ag_3PO_4 and Ag_2MoO_4 were calculated to be 0.285 and -0.125 eV, respectively. According to E_{VB} and E_{CB} values, the alignment of band energy level diagram and possible charge transfer process is illustrated in Figure 11. Under visible light irradiation, electrons are excited to CB, inducing the formation of holes at VB of both Ag_3PO_4 and Ag_2MoO_4. Meantime, the photoexcited holes in VB of Ag_2MoO_4 can be migrated to VB of Ag_3PO_4 due to its higher valence band edge potential The photogenerated electrons can be migrated from conduction band of Ag_2MoO_4 to conduction band of Ag_3PO_4 (see Figure 11). As it is noted that strong oxidation potential of holes at valence band of pure Ag_3PO_4 and Ag_2MoO_4 could directly oxidize MB, RhB and MO dye molecules. On other hand it has been reported that the E_{VB} of Ag_3PO_4 and standard redox potentials of $^{\bullet}OH$ /H_2O are 2.67 eV and 2.72 eV (vs NHE), respectively [56-57]. This suggests that the photogenerated holes on the VB of the Ag_3PO_4 could not react with H_2O to form $^{\bullet}OH$. However, the holes generate $^{\bullet}OH$ radicals due

to higher E_{VB} of Ag_2MoO_4. In other hand, $O_2^{\bullet-}$ radicals produced from CB of Ag_2MoO_4 have more potential of -0.125 eV than -0.046 eV *v*s NHE [58-59]. Finally, it could be explained that both holes and $O_2^{\bullet-}$ effectively take part in the degradation of dyes.

In general, the strong light absorption capability and high separation efficiency of electron-hole pairs are the main factors which deciding the photocatalytic activities. The Ag_2MoO_4-Ag_3PO_4 composites exhibit a strong visible light absorption (see Figure 4 (b)). From Table 3, it could be observed that 10 wt% Ag_2MoO_4-Ag_3PO_4 shows higher valence band edge potential which is about 2.67 eV is beneficial to strong oxidation for photocatalytic degradation of MB, RhB and MO. Also, it is reported that the recombination rate of electrons-holes is a crucial one and obviously related to its photocatalytic degradation. Since, the PL study can be correlated with photocatalytic degradation results. The lower PL intensity of pure Ag_3PO_4 and Ag_2MoO_4-Ag_3PO_4 composite photocatalysts follows the order of 10 wt% Ag_2MoO_4-Ag_3PO_4 > pure Ag_3PO_4 > 5 wt% Ag_2MoO_4-Ag_3PO_4 > 15wt% Ag_2MoO_4-Ag_3PO_4. This clearly demonstrates that Ag_2MoO_4 on Ag_3PO_4 promotes the efficient separation of electrons-holes, which ultimately reduces the electron-hole recombination, the similar kind of phenomena was observed by Yiming He et al., [60].

CONCLUSIONS

High efficiency new visible light driven Ag_2MoO_4-Ag_3PO_4 composite photocatalysts were successfully prepared using MoO_3 as precursor by simple solution based in-situ experimental process. The as-prepared Ag_2MoO_4-Ag_3PO_4 composite photocatalyst exhibited superior photocatalytic degradation efficiency than those pure Ag_3PO_4 and Ag_2MoO_4. This superior photocatalytic degradation may originate from efficient separation of photogenerated electron-hole between Ag_2MoO_4 and Ag_3PO_4. The reason for higher and faster degradation of cationic dyes were explained based on the Ag_2MoO_4-Ag_3PO_4 composite photocatalysts which

embrace the negative charges on the surface thus facilitating attraction of charges together. Moreover, Ag_2MoO_4-Ag_3PO_4 composite photocatalyst shows good stability and the mineralization of dyes also confirmed. On the basis of present study, Ag_2MoO_4-Ag_3PO_4 is efficient and highly stable photocatalyst system which is expected to be a new composites system useful to degrade industrial toxic dyes.

▪ AUTHOR INFORMATION

Corresponding author: acbose@nitt.edu, Tel +91-431-2503605, Fax +91 (431) 2500133

Notes

The authors declare no financial interest.

▪ ACKNOWLEDGEMENTS

The authors are thankful to The Director, National Institute Technology, Tiruchirappalli, Tamil Nadu, India. Authors thank Dr. Shamima Hussain, UGC-DAE Consortium for Scientific Research, Kalpakkam, Tamil Nadu, India for XPS characterization.

▪ REFERENCES

(1) Hu X. L, Li G. S, Yu J. C, *Langmuir.,* 2010**, 26**, 3031-3039.

(2) Kubacka A, Fernandez-Garcia M, *Chem. Rev.,* 2012**, 112,** 1555-1614.

(3) Tong H, Ouyang S, Bi Y, Umezawa N, Oshikiri M, Ye J. H, *Adv. Matter.,* 2012, **24,** 229-251.

(4) Fu H. B, Pan C. S, Yao W. Q, Zhu Y. F, *J. Phys. Chem. B.,* 2005, **109,** 22432-22439.

(5) Wu J. M, Zhang T. W, *J. Photochem. Photobiol. A: Chem.,* 2004, **162,** 171-177.

(6) Wu J. M, *Environ. Sci. Technol.,* 2007, **41,** 1723-1728.

(7) Konstantinou I. K, Albanis TA, *Appl. Catal. B.,* 2004, **49,** 1-14.

(8) Gerischer H, Heller A, *J. Phys. Chem.,* 1991**, 95,** 5261-5267.

(9) Zhaoyong L, Jiling L, Zheng Z, Yan J, Liu P, Wang C, Yang G, *ACS Nano.,* 2015**, 9**, 7256-7265.

(10) Lou Z, Huang B, Wang Z, Ma X, Zhang R, Zhang X, Qin X, Dai Y, Myung-Hwan W, *Chem. Mater.,* 2014, **26**, 3873-3875.

(11) Clovis A. L, Glenda C, David B. L, Anthony J. O, Darlene K. S, Lisa A.S, *Environ. Sci. Technol.,* 2000, **34**, 4754-4758.

(12) Niu M, Feng H, Lifeng C, Ping H, Yunlong Y, Yuansheng W, *ACS Nano.,* 2010, **4,** 681-688.

(13) Peng Y, Yan M, Chen Q, Fan C, Hai-Yan Z, An Wu X, *J. Mater. Chem. A.,* 2014**, 2**, 8517-8524.

(14) Miyauchi M, Nukui Y, Atarashi D, Sakai E, *ACS Appl. Mater. Interfaces.,* 2013, **5**, 9770-9776.

(15) Deo M, Shinde D, Yengantiwar A, Jog J, Hannoyer B, Sauvage X, More M, Ogale S, *J. Mater. Chem.,* 2012, **22,** 17055-17062.

(16) Chen C, Cai W, Long M, Zhou B, Wu Y, Wu D, Feng Y, *ACS Nano.,* 2010, **11,** 6425-6432.

(17) Wang W, Jun Wang Z, Xuanzhen W, Wei Li L, Ren Q, Gao W, Liang Y, Shim H, *Dalton Trans.,* 2014**, 43**, 6735-6743.

(18) Han M, Ting Sun Pei Yun T, Xiaofeng C, Kiang T, Man Siu T, *RSC Adv.,* 2013, **3**, 24964-24970.

(19) Huang H, Li D, Lin Q, Wenjuan Z, Yu S, Yibin C, Meng S, Xianzhi Fu, *Environ. Sci. Technolo.,* 2009, **43,** 4164 - 4168.

(20) Shasha Y, Yue X, Dandan Xu, Zhipeng Liu, Fei Zhao, Dejun W, Yanhong Lin, *New J. Chem.,* 2015, **39,** 2917-2924.

(21) Bo Chai, Xing W, *RSC Adv.,* 2015, **5,** 7589-7596.

(22) Li D, Xue J, Ma J, Tang J, *New J. Chem.,* 2016, **40,** 3330-3335.

(23) Yi Z, Jinhua Y, Kikugawa N, Kako T, Ouyang S, Stuart-Williams H, Yang H, Cao J, Luo W, Zhaosheng Li, Liu Y, Ray L. W, *Nat. Mater.,* 2010, **9,** 559-564.

(24) Umezawa N, Shuxin O, Jinhua Ye, *Phys. Rev B.,* 2011, **83,** 035202 (1-8).

(25) Guo J, Shuxin O, Zhou H, Kako T, Jinhua Ye, *J. Phys. Chem. C.,* 2013, **117**, 17716-17724.

(26) Lili Z, Hengchao Z, Hui H, Yang L, Zhenhui K, *New J. Chem.,* 2012, **36,** 1541-1544.

(27) Zheng-Mei Y, Gui-Fang H, Wei-Qing H, Jia-Mou W, Xin-Guo Y, Yue-Yang L, Chao J, Zhuo W, Anlian P, *J. Mater. Chem. A.,* 2014, **2,** 1750 -1756.

(28) Weifeng Y, Bo Zhang, Cunping H, Chao Ma, Xiulan S, Qunjie Xu, *J. Mater. Chem.,* 2012, **22,** 4050 - 4055.

(29) Fu G, Xu G, Chen S, Lei L, Zhang M, *Catal. Commun.,* 2013, **40,** 120-124.

(30) Jo Y. K, Kim I. Y, Lee J. M, Nahm S, Choi J. W, Hwang S. J, *Mater. Lett.,* 2014, **114,** 152-155.

(31) Zhankui C, Mengmeng S, Zhi Z, Liwei M, Wenjun F, Huimin J, *Catal. Commun.,* 2013, **42,** 121-124.

(32) Xiaofei Y, Haiying C, Yang Li, Jieling Qin, Rongxian Z, Hua T, *ACS Catal.,* 2013, **3,** 363-369.

(33) Dong P, Wang Y, Cao B, Xin S, Guo L, Zhang J, Li F, *Appl. Catal. B.,* 2013**, 132**, 45-53.

(34) Zhang H, Huang H, Ming H, Li H, Zhang L, Liu Y, Kang Z, *J. Mater. Chem.,* 2012, **22,** 10501-10506.

(35) Lei Liu, Jincheng Liu and Darren Delai Sun, *Catal. Sci. Techno.,* 2012, **2**, 2525-2532

(36) Yuyu Bu and Zhuoyuan Chen, *ACS Appl. Mater. Interfaces.,* 2014, **6**, 17589-17598

(37) Santhosh Kumar, Surendar, Arabinda Baruah, Vishnu S, *J. Mater. Chem. A.,* 2013, **1**, 5333-5340

(38) Neerugatti KrishnaRao E, Venktesh V. K, Praveen C.R, Giridhar M, *Ind. Eng. Chem. Res.,* 2015, **54,** 8031-8042.

(39) Zhihong C, Weilin W, Zhengguo Z, Xiaoming F, *J. Phys. Chem. C.,* 2013, **117**, 19346-19352.

(40) Hao J, Jin-Ku L, Jian-Dong W, Yi Lu, Xiao-Hong Y, *CrystEngComm.,* 2015, **17**, 5511-5521.

(41) Chithambararaj A, Sanjini N.S, Chandra Bose A, Velmathi S, *Catal. Sci. Technol.,* 2013, **3**, 1405-1414.

(42) Wanying Z, Gaiping L, Ping Y, Lifen Y, Lanqun M, *J. Phys. Chem. C.,* 2013, 117, 15183-15191.

(43) Bi Y, Ouyang S, Cao J, Ye J, *Phys. Chem. Chem. Phys.,* 2011, 13, 10071-10075.

(44) Bo C, Jing Li, Qian Xu, *Ind. Eng. Chem., Res.* 2014, 53, 8744-8752**.**

(45) Saravanamoorthy S, Chandra Bose A and Velmathi S, *RSC adv.,* 2015, **5**, 99074-99083.

(46) Muhammad T, Chuanbao C, Nasir Mahmood, Faheem K. Butt, Asif Mahmood, Faryal I, Sajad Hussain, Tanveer M, Zulfiqar A, Imran Aslam, *ACS Appl. Mater. Interfaces.,* 2014, **6,** 1258-1265.

(47) Li X.Z, Li X.Z, *Environ. Sci. Technol.,* 2001, **35,** 2381-2387.

(48) Peng T. Y, Li K, Zeng P, Zhang Q. G, Zhang X. G, *J. Phys. Chem. C.,* 2012**, 116**, 22720-22726.

(49) Wen Qian, P. Alex Greaney, Simon Fowler, Sheng-Kuei Chiu, Andrea M. Goforth, and Jun Jiao, *ACS Sustainable Chem. Eng.,* 2014, **2,** 1802-1810.

(50) Xiaoyan J, Young Kim I, Yun Kyung Jo, Jerry L. Bettis, Hyun-Joo K, Myung-Hwan Whangbo Jr, Seong-Ju H, *J. Phys. Chem. C.,* 2013, **117,** 26509-26516.

(51) Mrinmoyee B, Arun Kumar Sinha, Mukul Pradhan, Sougatasarkar, Yuichinegishi, Govind, Tarasankar Pal, *Environ. Sci. Technol.,* 2010, **44,** 6313-6318.

(52) Ming Ge, Zhu Na, Yaping Zhao, Jing Li, Lu Liu, *Ind. Eng. Chem. Res.,* 2012, **51**, 5167-5173.

(53) Xiaomeng W, Shaogui Yang, Hui Li, Wei Zhao, Cheng S, Huan He, *RSC Adv.,* 2014, **4**, 42530-42357.

(54) Jian T, Yuanhua S, Zhenhuan Z, Weijia Z, Dongzhou W, Xueliang K, Hong Liu, Jiyang W, Shaowei C, Huaqiang C, Hui Huang, *Small.,* 2013**, 9 (22),** 3864-3872.

(55) Mingce L, Weimin C, *Nanoscale.,* 2014, **6,** 7730-7742.

(56) Cao J, Luo B. D, Lin H. L, Xu B. Y, Chen S. F, *J. Hazard. Mater.,* 2012, **107-115**, 217-218.

(57) Ma X. G, Lu B, Li D, Shi R, Pan C. S, Zhu Y. F, *J. Phys. Chem. C.,* 2011, **115,** 4680-4687.

(58) Hongwei Huang, Ying He, Xiaowei Li, Min Li, Chao Zeng, Fan Dong, Xin Du, Tierui Zhang and Yihe Zhang, *J. Mater. Chem. A.,* 2015, **3**, 24547-24556.

(59) Liqun Ye, Jinyan Liu, Zhuo Jiang, Tianyou Peng and Ling Zan, *Appl. Catal. B,* 2013, **142**, 1-7

(60) Yiming H, Lihong Z, Botao T, Maohong F, *Environ. Sci. Technol.,* 2015, **49,** 649-656.

Figure captions:

Figure 1. XRD patterns of pure Ag_3PO_4, 5 wt% Ag_2MoO_4-Ag_3PO_4, 10 wt% Ag_2MoO_4-Ag_3PO_4, 15 wt% Ag_2MoO_4-Ag_3PO_4 and pure Ag_2MoO_4

Figure 2. XPS spectra of the as-synthesised 10 wt% Ag_2MoO_4-Ag_3PO_4 (a) XPS survey spectrum (b) Ag (3d) spectrum (c) Mo (3d) spectrum (d) P (2p) spectrum (e) O (1s) spectrum

Figure 3. SEM images of (a) pure Ag_3PO_4 (b) pure Ag_2MoO_4 (c) 10 wt% of Ag_2MoO_4-Ag_3PO_4 composite

Figure 4. (a) FTIR spectra (b) UV-vis diffuse reflectance spectra (c) Bandgap (d) Photoluminescence spectra of pure and Ag_2MoO_4-Ag_3PO_4 composite

Figure 5. Zeta potential measurement of Ag_2MoO_4-Ag_3PO_4 composite

Figure 6. Self photolysis of MB, RhB and MO under visible light irradiation

Figure 7. Photodegradation of MB (a) pure Ag_3PO_4 (b) 5 wt% Ag_2MoO_4-Ag_3PO_4 (c) 10 wt% Ag_2MoO_4-Ag_3PO_4 (d) 15 wt% Ag_2MoO_4-Ag_3PO_4 composite photocatalyst and (e) pure Ag_2MoO_4

Figure 8. Photocatalytic activity of (a) pure Ag_3PO_4, pure Ag_2MoO_4 and Ag_2MoO_4-Ag_3PO_4 composites for MB degradation (b) RhB and MO degradation using 10 wt% Ag_2MoO_4-Ag_3PO_4 composite

Figure 9. Interaction between dye molecules (cationic and anionic) and Ag_2MoO_4 - Ag_3PO_4 composite

Figure 10. (a) Reactive species trapping experiments on the MB degradation over 10 wt% Ag_2MoO_4-Ag_3PO_4 (b) recyclability experiment of 10 wt% Ag_2MoO_4-Ag_3PO_4 composite (c) XRD pattern of 10 wt% Ag_2MoO_4-Ag_3PO_4 before and after the photocatalytic degradation of MB (d) FTIR spectra of dyes before degradation (i) MB, (iii) RhB (v) MO powder and (ii), (iv), (vi) after photocatalytic reaction

564 **Figure 11.** Schematic representation of band energy levels of Ag_2MoO_4-Ag_3PO_4 composite
565 under visible light irradiation
566
567
568
569
570
571
572
573
574
575
576
577
578
579
580
581
582
583
584
585
586
587
588

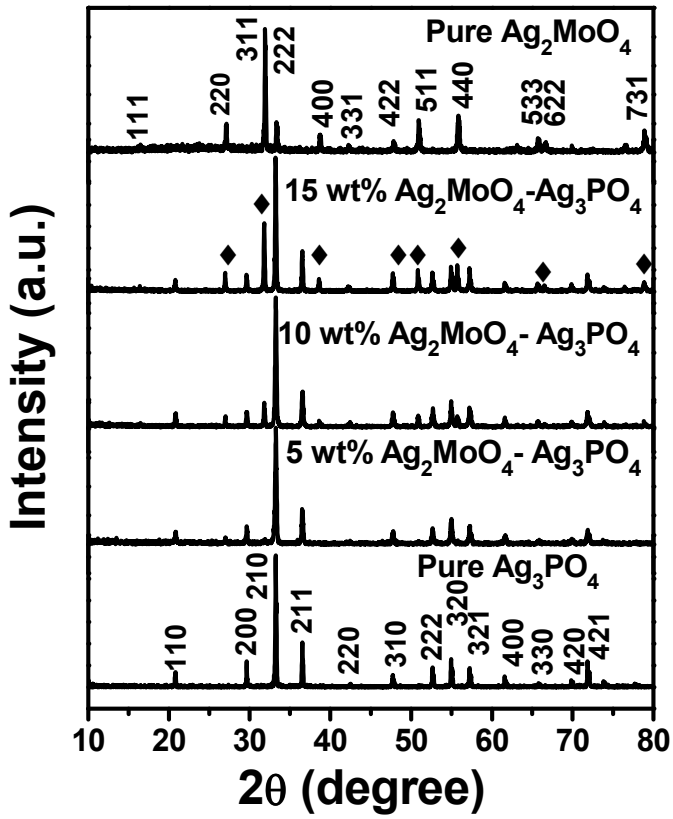

Figure 1. XRD patterns of pure Ag_3PO_4, 5 wt% Ag_2MoO_4- Ag_3PO_4, 10 wt% Ag_2MoO_4- Ag_3PO_4, 15 wt% Ag_2MoO_4- Ag_3PO_4 composites and pure Ag_2MoO_4 (♦- Indicates Ag_2MoO_4 phase).

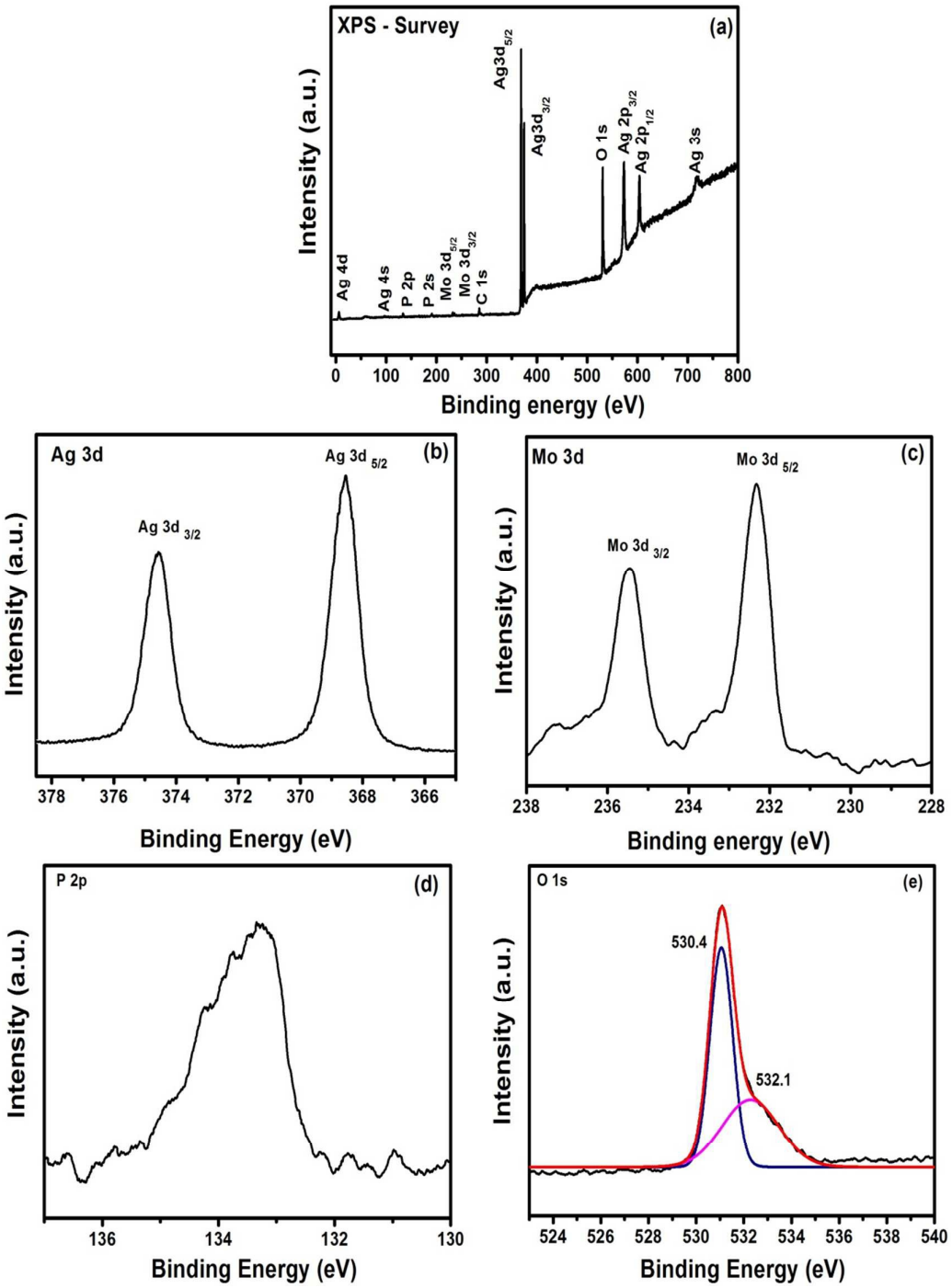

Figure 2. XPS spectra of the as-synthesised 10 wt% Ag_2MoO_4-Ag_3PO_4: (a) XPS survey spectrum; (b) Ag (3d) spectrum; (c) Mo (3d) spectrum; (d) P (2p) spectrum; (e) O (1s) spectrum;

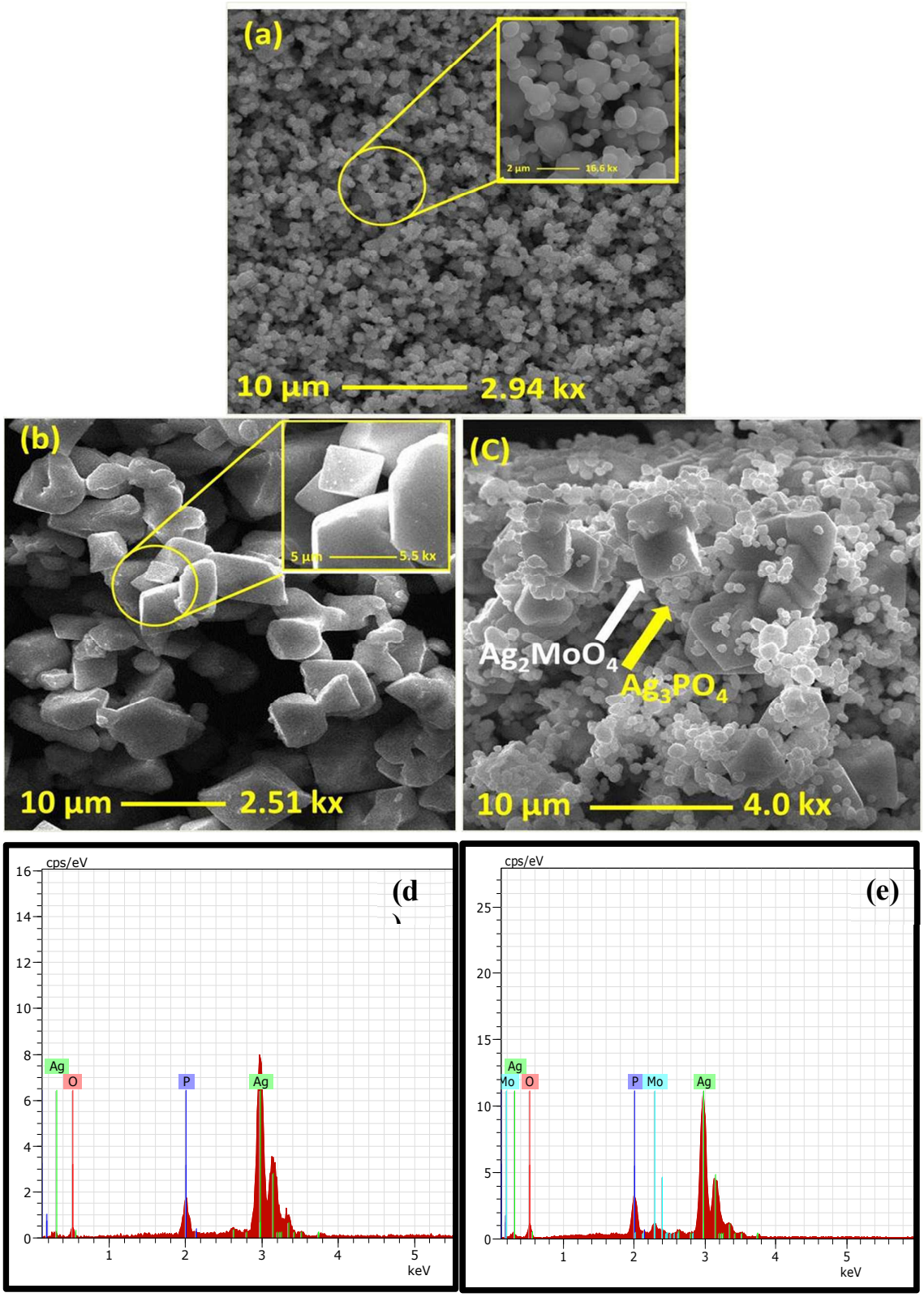

Figure 3. SEM images of (a) pure Ag_3PO_4, (b) pure Ag_2MoO_4 (c) 10 wt% Ag_2MoO_4-Ag_3PO_4 composites.

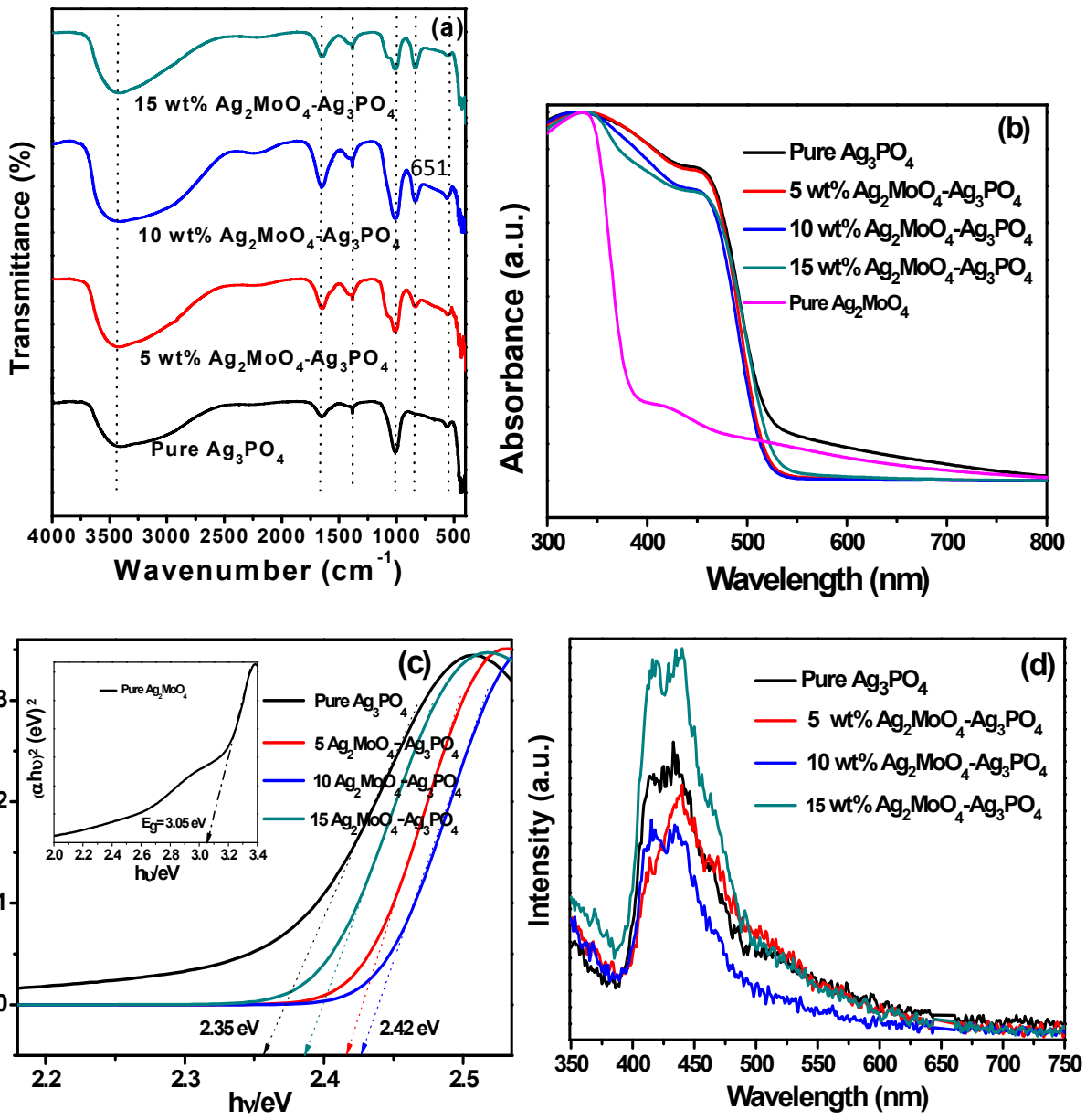

Figure 4. (a) FTIR spectra pure Ag_3PO_4 and Ag_2MoO_4-Ag_3PO_4 composites (b) UV- vis diffuse reflectance spectra pure Ag_3PO_4, pure Ag_2MoO_4 and Ag_2MoO_4-Ag_3PO_4 composites (c) Bandgap and (d) Photoluminescence spectra of pure Ag_3PO_4 and Ag_2MoO_4-Ag_3PO_4 composites

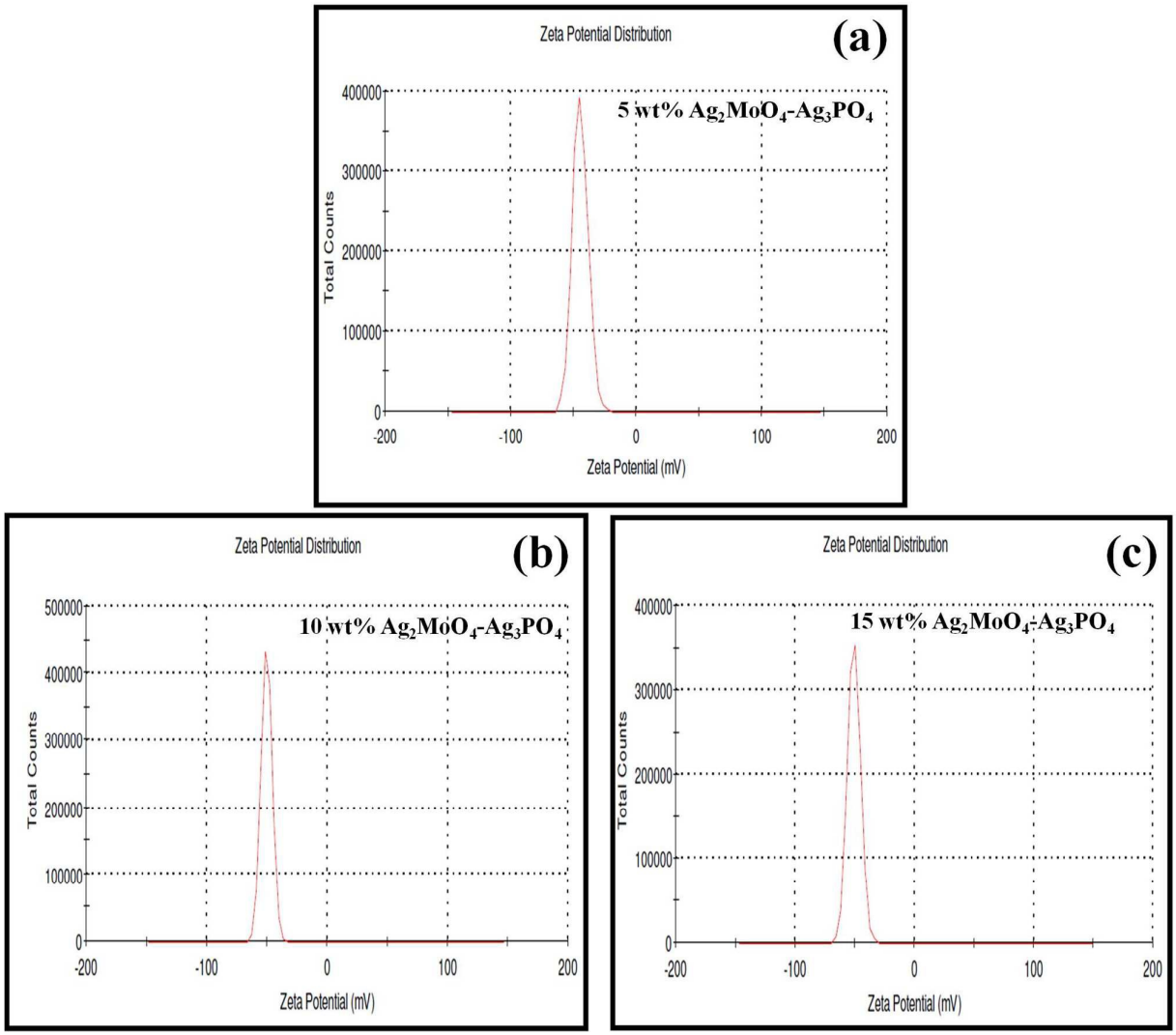

Figure 5. Zeta potential measurement of (a) 5wt% Ag_2MoO_4-Ag_3PO_4 (b) 10wt% Ag_2MoO_4-Ag_3PO_4 and (c) 15 wt% Ag_2MoO_4-Ag_3PO_4 composites

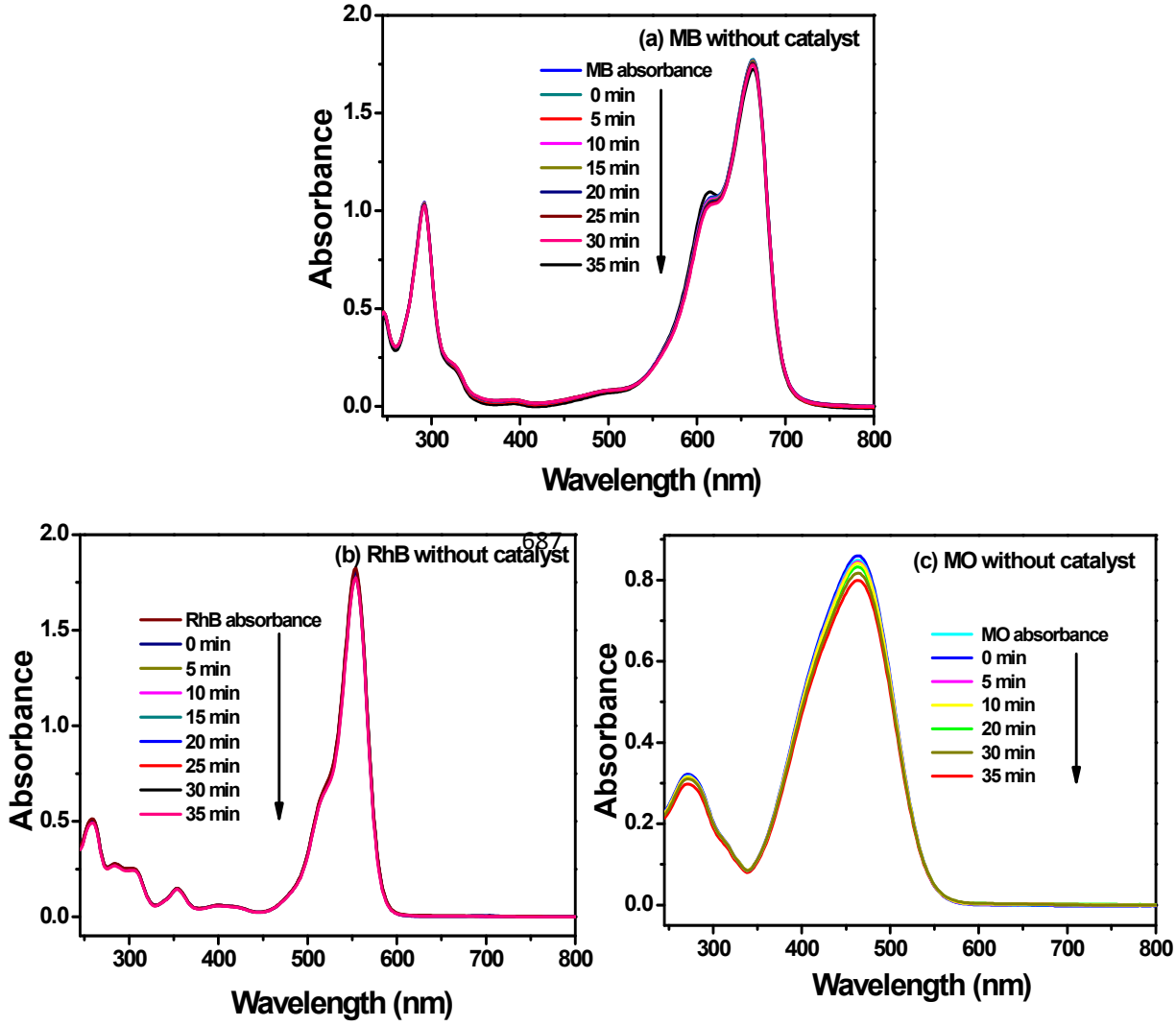

Figure 6. Self photolysis of MB, RhB and MO under visible light irradiation

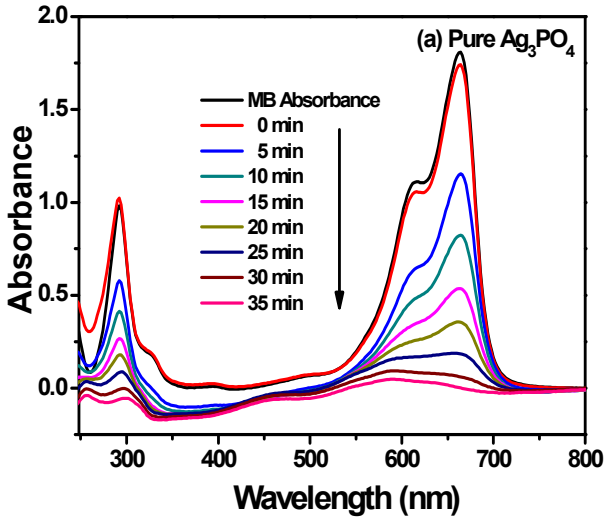

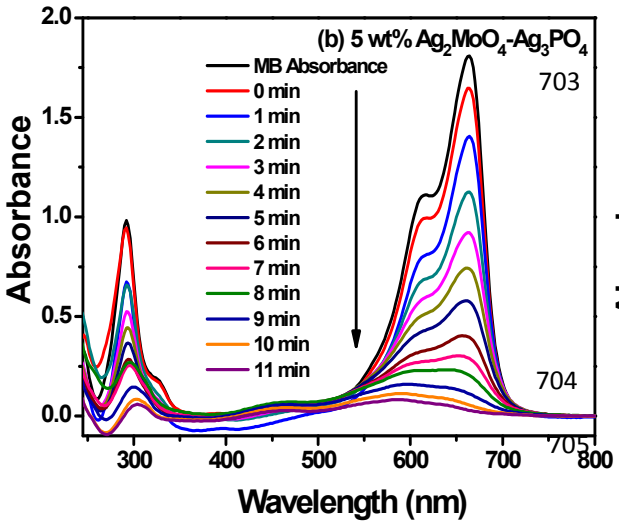

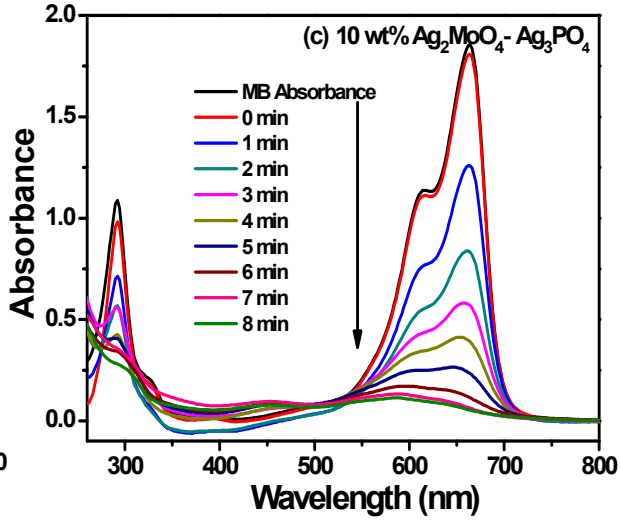

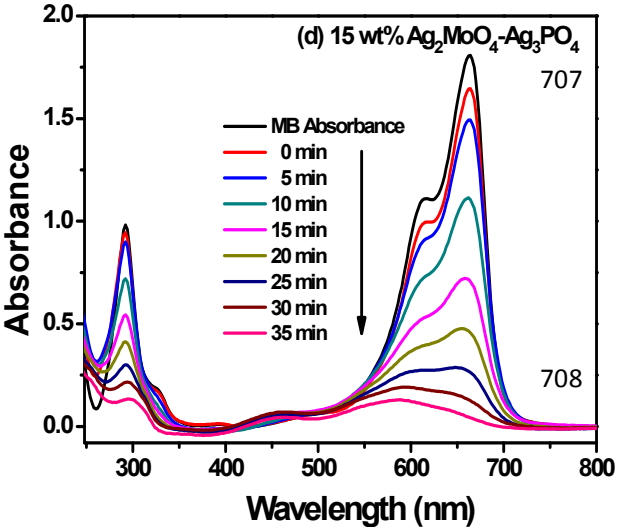

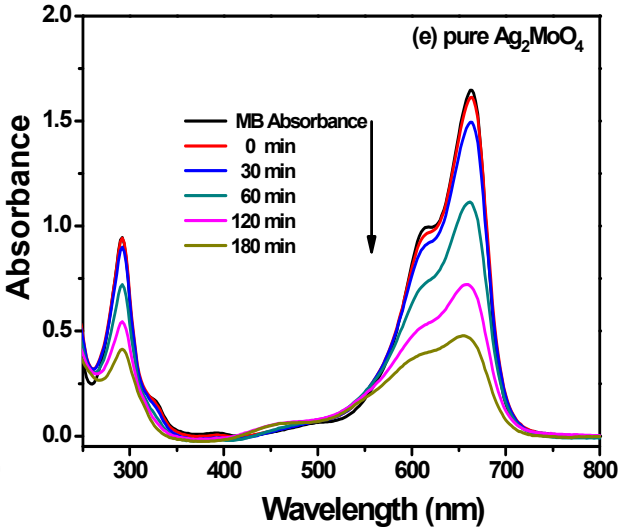

Figure 7. Photodegradation of MB (a) pure Ag_3PO_4, (b) 5 wt% Ag_2MoO_4-Ag_3PO_4 (c) 10 wt% Ag_2MoO_4-Ag_3PO_4 (d) 15 wt% Ag_2MoO_4-Ag_3PO_4 composite photocatalyst and (e) pure Ag_2MoO_4

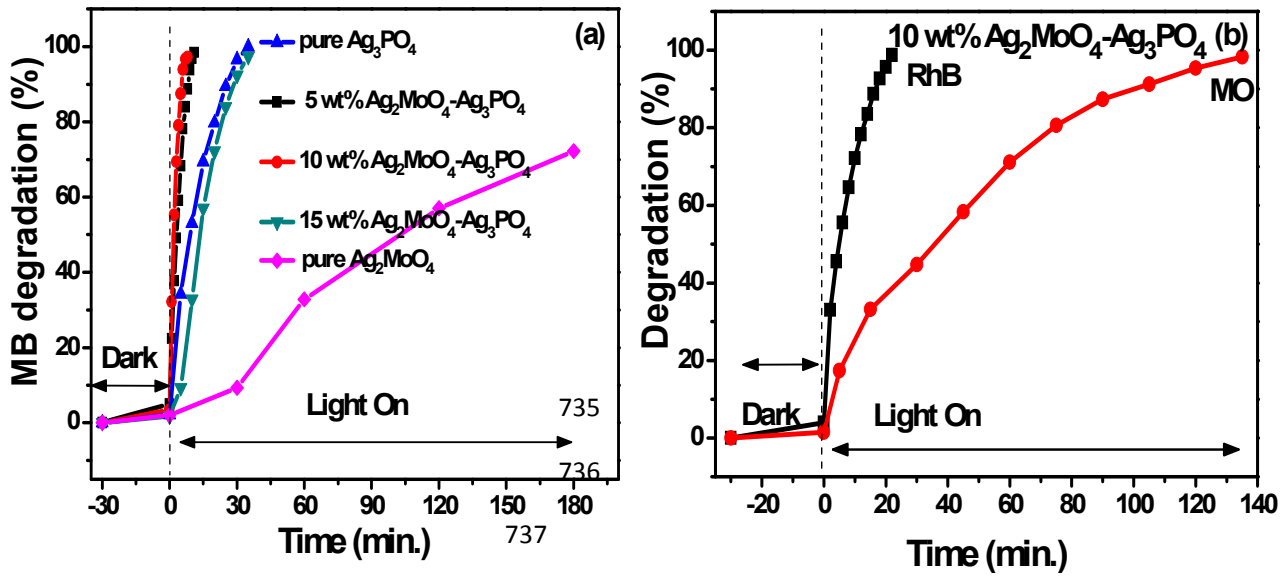

Figure 8. Photocatalytic activity of (a) pure Ag_3PO_4, pure Ag_2MoO_4 and Ag_2MoO_4-Ag_3PO_4 composites for MB degradation (b) RhB and MO degradation using 10 wt% Ag_2MoO_4-Ag_3PO_4 composite

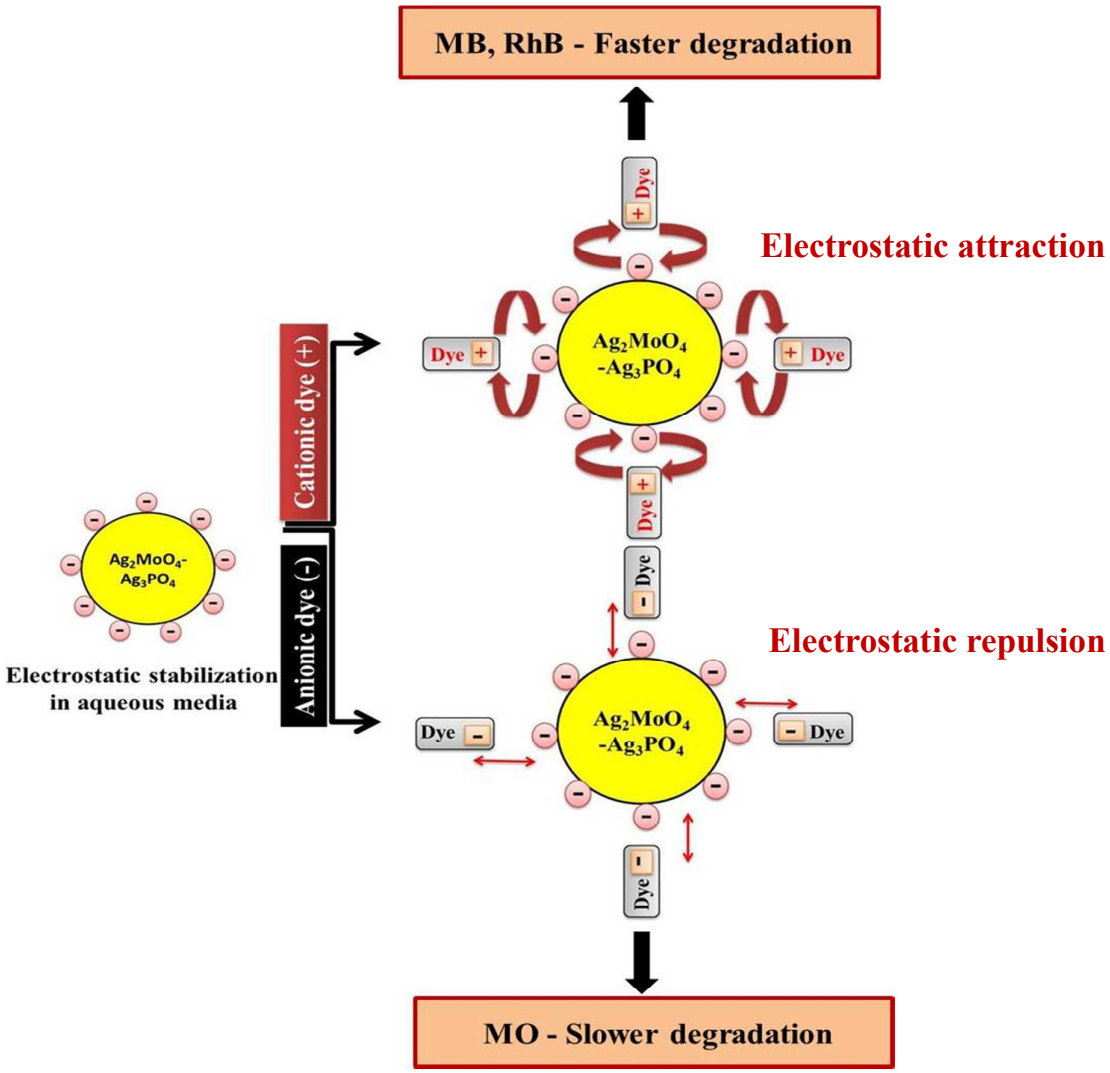

Figure 9. Interaction between dye molecules (cationic and anionic) and Ag_2MoO_4-Ag_3PO_4 composite

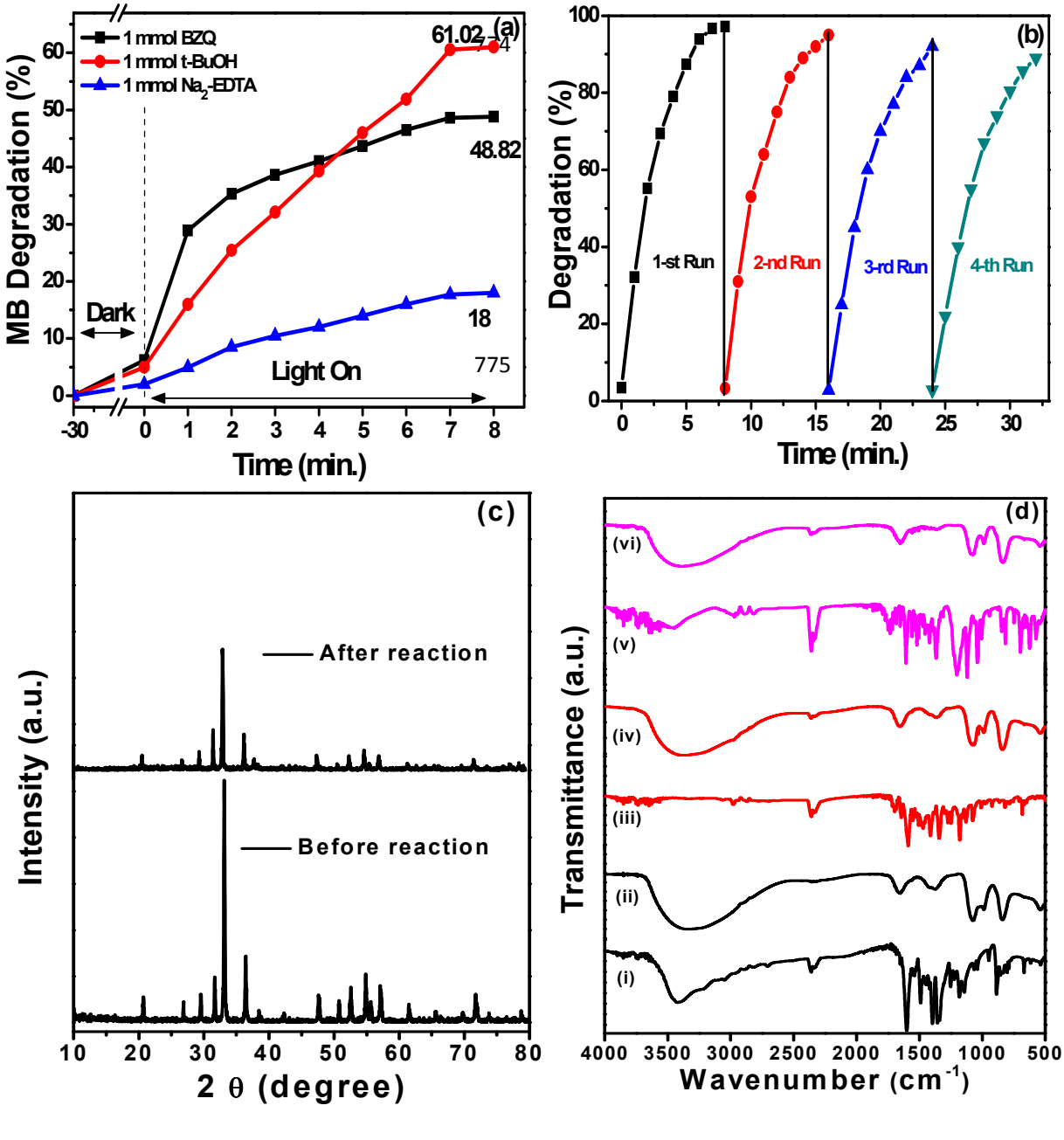

Figure 10. (a) Reactive species trapping experiments on the MB degradation over 10 wt% Ag_2MoO_4-Ag_3PO_4 composite (b) recyclability experiment of 10 wt% Ag_2MoO_4-Ag_3PO_4 composite (c) XRD pattern of 10 wt% Ag_2MoO_4-Ag_3PO_4 composite before and after the photocatalytic reaction of MB (d) FTIR spectra of dyes before degradation (i) MB, (iii) RhB, (v) MO powder and (ii), (iv), (vi) after photocatalytic reaction.

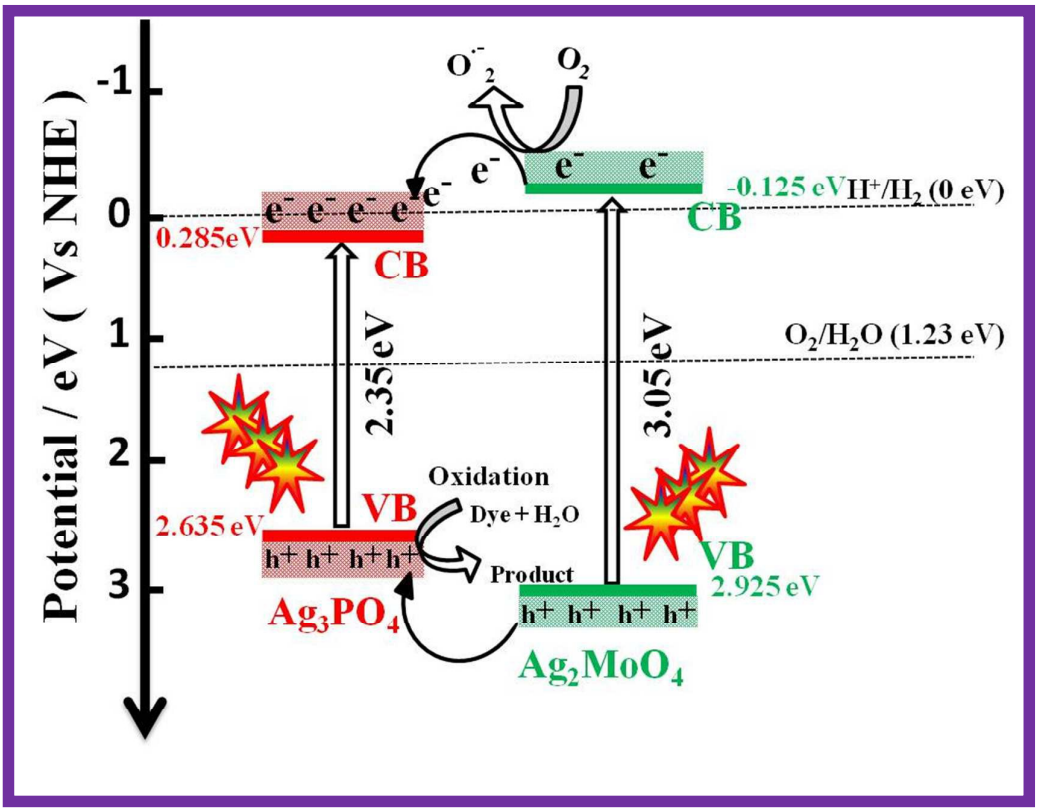

Figure 11. Schematic representation of band energy levels of Ag_2MoO_4-Ag_3PO_4 composite under visible light irradiation.

Table 1. Elemental composition of pure Ag_3PO_4

Element	Weight %	Atomic %
O K	14	47.94
Ag L	79.34	40.29
P K	6.66	11.77
Total (%)	100	100

Table 2. Elemental composition of 10 wt% Ag_2MoO_4-Ag_3PO_4 composite

Element	Weight %	Atomic %
O K	22.66	61.16
Ag L	64.88	25.97
P K	7.69	10.72
Mo L	4.77	2.15
Total (%)	100	100

843

844

845 **Table 3. The calculated Bandgap (E_g), valence band edge potential (E_{VB}) and conduction**
846 **band edge potential (E_{CB}) of pure Ag_3PO_4, Ag_2MoO_4-Ag_3PO_4 composites and pure**
847 **Ag_2MoO_4.**

Sample Name	Pure Ag_3PO_4	5wt%Ag_2MoO_4 -Ag_3PO_4	10wt%Ag_2MoO_4 -Ag_3PO_4	15wt%Ag_2MoO_4 -Ag_3PO_4	Pure Ag_2MoO_4
E_g (eV)	2.35	2.41	2.42	2.38	3.05
E_{VB} (eV)	2.63	2.66	2.67	2.65	2.92
E_{CB} (eV)	0.28	0.25	0.25	0.27	-0.12

848

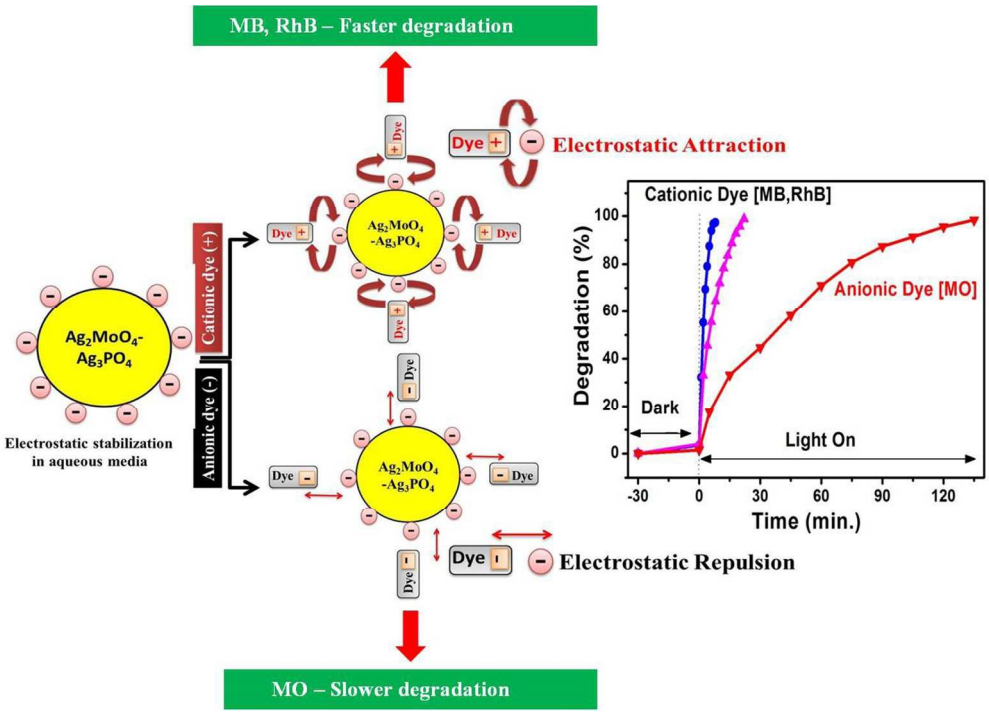

Interaction between dyes and Ag2MoO4-Ag3PO4 composites

230x162mm (150 x 150 DPI)